Optica Applicata, Vol. XIII, No. 4, 1983

Preliminary results of the heterodyne measurements of weak 10.6 μm signals with room-temperature HgCdTe photodetectors*

MIROSŁAW KOPICA, MAREK STRZELEC, ZDZISŁAW TRZĘSOWSKI

Institute of Quantum Electronics, Military Academy of Technology, Warszawa-Bemowo, Poland.

We have studied several parameters of uncooled infrared detectors in coherent detection. We present here the well known theoretical relations for noise and signals in heterodyne detection process as well as experiments performed at 10.6 μm with room-temperature HgCdTe photoresistors. We have studied the relations between the magnitude of heterodyne signal and local oscillator power and the possibility of achieving near theoretical limit in heterodyne detection with these room-temperature detectors. In a simple and not optimal configuration we have detected Doppler infrared signals of 10^{-11}[W]. This technique might prove useful for infrared heterodyne spectroscopy, pollution monitoring, laser Doppler velocimetry and infrared radar.

1. Introduction

There exist two basic detection techniques: direct (incoherent) and optical mixing (coherent or heterodyne) one.

The first technique (Fig. 1) is the simplest one even for coherent laser radiation. The lens system and photodetector are to detect the instantaneous power in the collected field as it arrives at the receiver. Such receivers can be

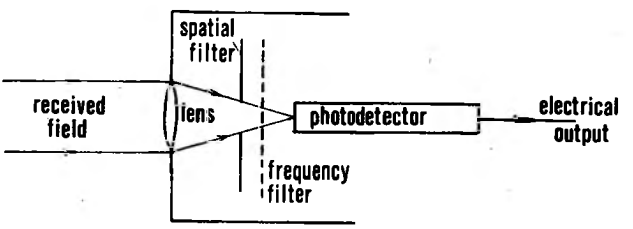

Fig. 1. Direct detection receiver

used wherever the transmitted information appears in the form of power variation of the received field. In this detection technique all information about the frequency and phase is lost.

---

* This paper has been presented at the European Optical Conference (EOC'83), May 30–June 4, 1983, in Rydzyna, Poland.

Heterodyne detection system is shown in Figure 2. In optical mixing, a signal carrier of frequency ω_S is combined with a stable coherent optical local oscillator of frequency ω_{LO} with a beam-splitter. They both are then directed towards the input of a photodetector, where the action of mixing takes place, because detectors respond to the square of the sum of the signal and local oscillator fields. The resulting output signal is of the intermediate frequency $|\omega_S - \omega_{LO}|$.

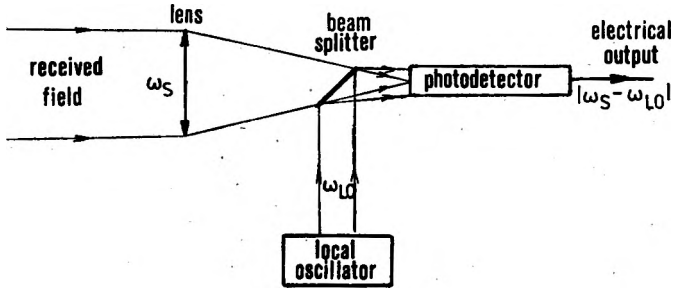

Fig. 2. Heterodyne detection receiver

Such receivers are used whenever optical information is amplitude, frequency or phase-modulated.

Heterodyne detection allows the realization of optical receivers with high sensitivity, almost to the theoretical quantum-noise limit. This is attainable in a well designed optical heterodyne receiver, where the noise is dominated by local oscillator induced noise.

2. Signal to noise ratio in coherent detection

In our consideration we take into account amplifier noise which is characterized by the noise figure F. We define it (Fig. 3) as follows:

$$F = (S/N)_{IN}/(S/N)_{OUT} \tag{1}$$

where S and N represent the electrical signal and noise powers, respectively, with the same resistor R_D at a temperature of 300 K. The gain G of the amplifier takes into account any mismatch between the load R_D and the amplifier input

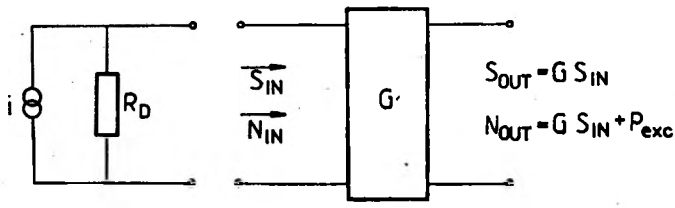

Fig. 3. Detector amplifier circuit

impedance [1, 2]. Taking P_{exc} as the excess noise added by the amplifier, the effective thermal input noise becomes

$$(N_{\text{IN}})_{\text{eff}} = \frac{N_{\text{OUT}}}{G} = kT_{\text{eff}}B \tag{2}$$

where $T_{\text{eff}} = T_D + (F-1)T_{300}$, (3)

(T_D – detector temperature, B – detection bandwidth).

To calculate the power signal to noise ratio at the output of the detector, we take into account *heterodyne* current of intermediate frequency $\omega_{IF} = \omega_S - \omega_{LO}$:

$$\overline{i_{IF}^2} = 2i_{LO}i_S, \tag{4}$$

and noise current

$$\overline{i_N^2} = 2e(i_S + i_{LO} + i_B + i_D)BNg \tag{5}$$

where: i_S, i_{LO}, i_B, i_D – signal, local oscillator background and dark currents, respectively,

e – electron charge,

g – internal current gain factor,

$N = 1$ for reverse biased photodiodes,

$N = 2$ for generation-recombination limited photoconductors and unbiased photodiodes.

For the heterodyne detection we use i_{IF} as the signal current and write the signal to noise ratio as

$$(S/N)_{\text{OUT}} = \frac{\overline{i_{IF}^2}}{\overline{i_N^2} + \dfrac{4kT_{\text{eff}}B}{R_D}}. \tag{6}$$

Taking into account a sufficiently high local oscillator power, when noise due to signal, background and dark current becomes small, we obtain finally

$$(S/N)_{\text{OUT}} = \frac{P_S}{NhvB\left[1 + \left(\dfrac{hv}{e}\right)\left(\dfrac{kT_{\text{eff}}}{e}\right)\left(\dfrac{2}{N\eta g^2 R_D P_{LO}}\right)\right]}. \tag{7}$$

The theoretical quantum-noise limit or ideal heterodyne detection can be achieved if

$$P_{LO} \geqslant \left(\frac{hv}{e}\right)\left(\frac{kT_{\text{eff}}}{e}\right)\left(\frac{2}{N\eta g^2 R_D}\right). \tag{8}$$

The physical significance is that the noise due to the total power falling on the detector dominates over the excess noise generated in the following amplifiers.

The expression (8) indicates that the photodetector is useful for heterodyne detection if the term $N\eta g^2 R_D$ is suitably large.

Next, we can see that for the heterodyne detection two cases may occur:

i) for strong P_{LO} powers

$$P_{LO} \geqslant P_K$$

where

$$P_K = \frac{h\nu}{e} \frac{kT_{\text{eff}}}{e} \frac{1}{\eta g^2 R_D},$$

and

$$(S/N)_{\text{OUT}} \cong \frac{P_S}{2h\nu B}$$

as in the case of quantum-noise-limited detector;

ii) for $P_{LO} \leqslant P_K$.

In our experiment we use uncooled HgCdTe photoresistors manufactured in Institute of Plasma Physics, Warsaw (Poland). Taking into account that $i_S/i_{LO} \leqslant 1$ and $i_B/i_{LO} \leqslant 1$ and using equations (4)–(6), we obtain for this detector

$$(S/N)_{\text{OUT}} = \frac{i_S}{2eBg\left[1 + \frac{i_D}{i_{LO}} + \left(\frac{kT_{\text{eff}}}{eR_D g}\right)/i_{LO}\right]}, \tag{9}$$

or

$$(S/N)_{\text{OUT}} = \frac{\eta P_S}{2h\nu B} \frac{1}{1 + \frac{P_D + P_K}{P_{LO}}}. \tag{10}$$

For typical detector parameters: $R = 50\Omega$, $g = 10^{-2}$, $\eta = 0.1$, $T_D = 300$ K, $N = 2$, $i_D = 0.1$ [A], $F = 5$, $B = 5$ [MHz], we obtain

$$(S/N)_{\text{OUT}} = \frac{\eta P_S}{2h\nu B} \frac{1}{1 + \frac{43}{P_{LO}}}. \tag{11}$$

Damage levels for this photoresistor are of 10^2 [W/cm^2] for cw optical input power and 10^6 [W/cm^2] for short laser pulses. It can be seen that the near theoretical quantum-noise limit is obtained solely with pulsed local oscillator. Our experiments, described in this paper, were performed in the region of $P_{LO} \leqslant P_K + P_D$, and then signal to noise ratio was a linear function of P_{LO}.

3. Experiments

A block diagram of the preliminary experimental arrangement used for the heterodyne measurements in photoresistive HgCdTe at 300 K is shown in Fig. 4. In this laboratory setup, similar to the arrangement shown in [3] we employed a conventional sealed-off CO_2 laser, with an output power of approximately 4 W at 10.6 μm. It used external output germanium mirror and diffraction

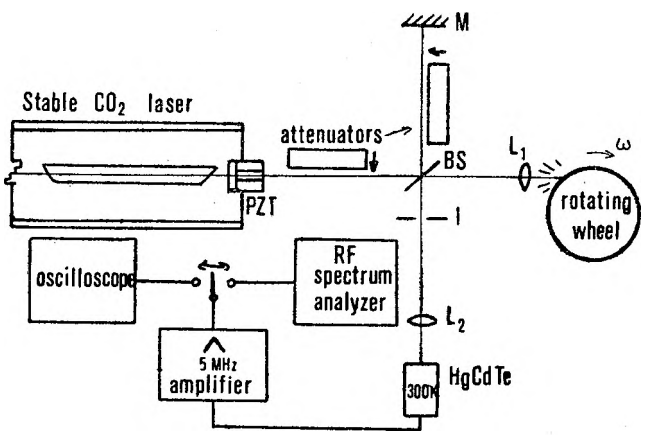

Fig. 4. Experimental arrangement for heterodyne measurements

grating, with plasma tube closed off by salt windows oriented at Brewster angle. The cavity length was held constant by use of four invar spacing rods between the mirror holders. This minimized frequency drifting due to thermal changes. A variable beam-limiting aperture was placed in front of the spherical output mirror resulting in the desired fundamental TEM_{00} mode. The output mirror was mounted on a piezoelectric transducer arranged to control the length of the laser cavity, thus allowing control of the laser frequency. An active *dither* stabilization scheme can be applied to this configuration resulting in better than 10^8 long-term frequency stability.

The CO_2 laser served as a source of radiation for both, measurement and local oscillator waves in a classical interferometer configuration. One mirror of the conventional interferometer was replaced by an off-centre rotating, sand-blasted aluminum wheel. The diffusely scattered radiation from the wheel provided a Doppler-shifted signal which was recombined at the beam-splitter (*BS*) with the unshifted local oscillator (*LO*) radiation reflected from the mirror (*M*). The mirror (*M*) was locked at a slight angle to the usual 90° in order to prevent this reflected radiation from feeding back into the laser.

The experimental setup was mounted on a granite slab. It was not isolated from vibrations, but it has been found that they were not coupled with the desired laser stability in the observation time interval. The laser was operated well above the threshold being, however, very carefully tuned to operate on a single line and mode, so that no excess noise was expected from the beam. This

was accomplished by adjusting laser mirrors and iris diaphragm in laser resonator for a TEM_{00} mode and the absence of any observable beat signal. The local oscillator mirror (M) was then adjusted to give the largest signal to noise ratio for signal beam. The detector was also carefully positioned and the procedure was repeated until such a mirror position was found for which all of the above conditions were coincident.

An uncoated Irtran 2 (ZnS) flat of thickness of 0.2 cm served as a beam-splitter (BS), and mirror (M) was standard gold coated glass. A salt NaCl lens L_1 of focal length of 5 cm was inserted in the signal beam to focus the radiation to a single point on the sandblasted rim of the rotating wheel. This lens served to collect sufficiently of scattered radiation to permit an incoherent direct measurement of the scattered signal power for calibration purposes. It also ensured spatial coherence of the scattered radiation over the receiver aperture. An iris I was used to maintain the angular alignment of the wavefronts of the two beams. The detector was fed through a low-noise wide-band amplifier to an oscilloscope or a spectrum analyzer.

The maximum local oscilloscope power, as determined by the reflectivity of the Irtran 2 flat, was about 0.3 W. It could be increased by a factor of ten by replacing the rotating wheel and detector in the interferometer's legs. In this last configuration it was necessary to keep detector below its damage threshold by chopping the incident laser power.

A photograph of the experimental equipment is shown in Fig. 5.

The mercury-cadmium-telluride R 005 detectors used in the heterodyne experiments were fast detectors optimized for 8–12 μm spectral region. Detailed specifications are shown in Table [4].

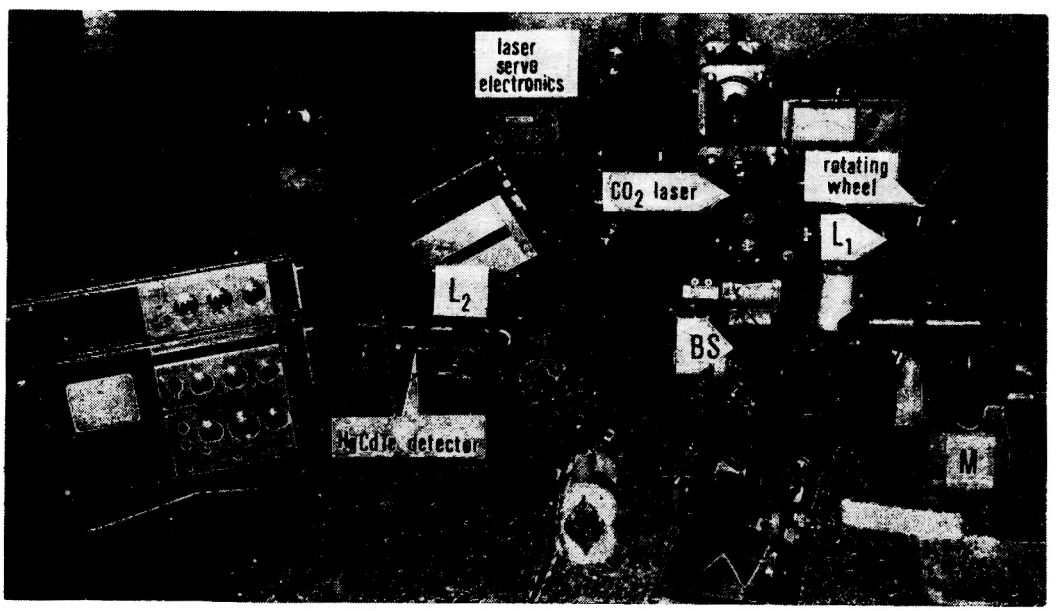

Fig. 5. Photograph of the heterodyne apparatus

It should be noted that R 005 detectors were not optimized for the heterodyne detection. Most of their applications include fast laser pulse diagnostics, high temperature plasma investigations and laser frequency control.

Specifications R 005 photoresistor		
Active area	mm^2	1×1
Responsivity	mV/W	10–100
Detectivity (10.6 μm, 10^8 Hz, 1Hz)	$cmHz^{1/2}/W$	$1\text{–}10 \times 10^6$
Rise time	ns	1
Maximum signal	V	1
Bias current	mA	100
Temperature	K	300

Figure 6 shows a multiple-sweep display of the heterodyne signal obtained at the detector output. The loss of definition of the wave form in the sixth cycle reflects the finite bandwidth of the heterodyne signal.

Figure 7 shows a single trace of this signal for a longer time scale. The modulation bandwidth is caused by statistical fluctuations of the heterodyne signal arising from the moving diffuse surface of the wheel.

The results of typical experimental measurements of the heterodyne signal for selected R 005 detectors are shown in Fig. 8. The circles and crosses represent the observed heterodyne power data points normalized to the 1 Hz bandwidth,

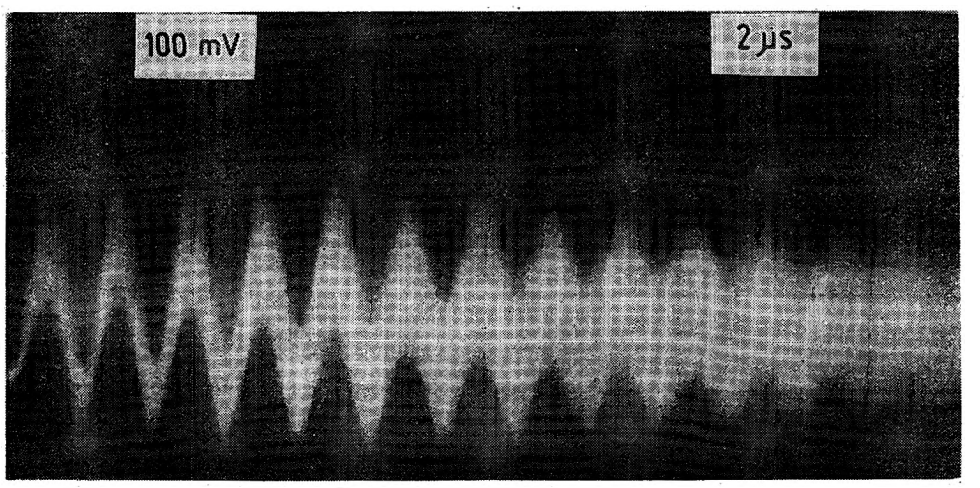

Fig. 6. A multiple-sweep display of the heterodyne signal

as a function of the product of signal beam radiation power and local oscillator power, $P_S \times P_{LO}$. Various values of $P_S \times P_{LO}$ were obtained by inserting calibrated germanium attenuators at the output of the CO_2 laser. The unattenuated signal power was measured by chopping the signal beam in the absence of the local oscillator power. As indicated earlier, the presence of L_1 lens facilitated this measurement. A plot of the theoretically expected results (relation (10)) for detector No. 1217 is also shown in Fig. 8. Using an estimated quantum efficiency of $\eta = 0.12$ it is seen to be in good agreement with the experimental

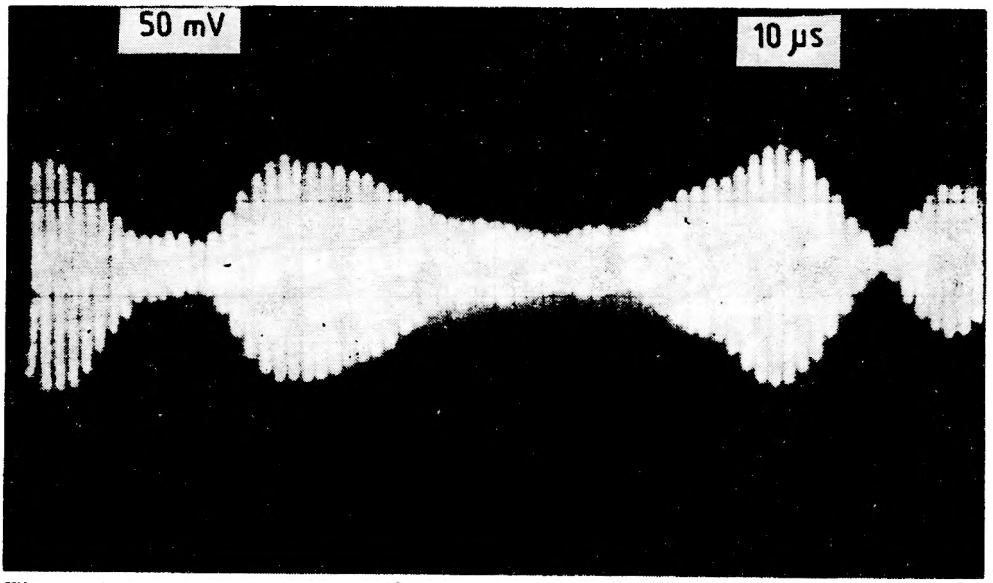

Fig. 7. A single-sweep heterodyne signal with a longer time scale

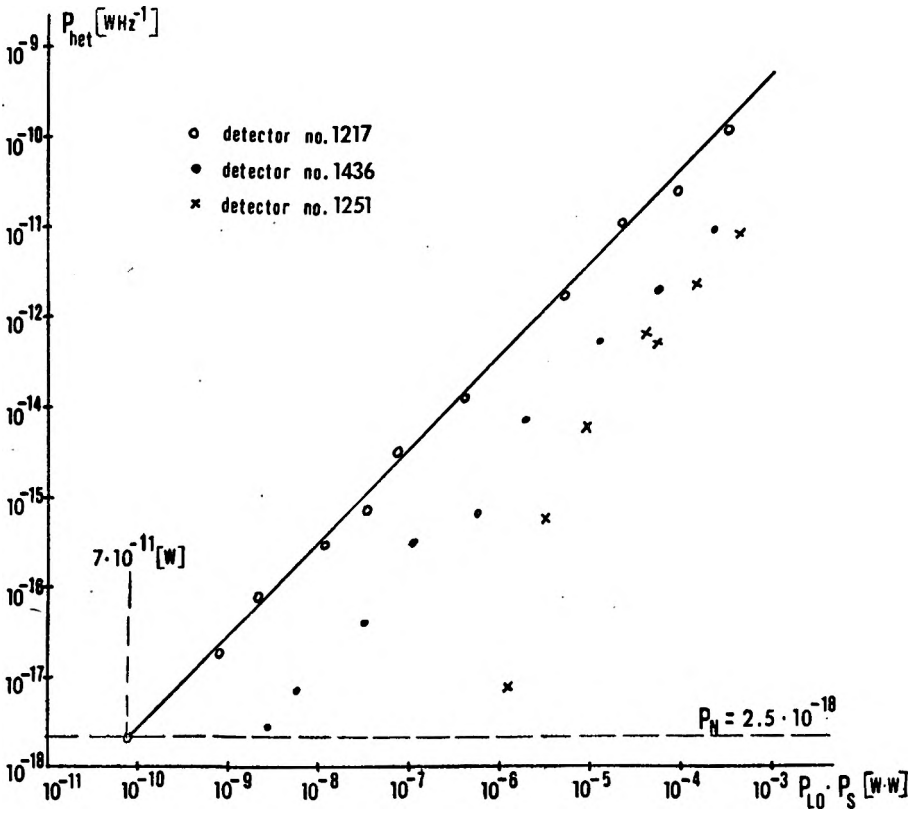

Fig. 8. The data points, obtained from a typical run, represent the observed and normalized heterodyne power for a given signal and local oscillator powers

data. The dashed horizontal line represents the noise power in this experiment. For detector No. 1217 and No. 1436 it is the amplifier noise.

We have observed an anomalous behaviour of detector No. 1251. As is shown in Fig. 8, the heterodyne signal for this detector does not show linear characteristic. This problem has not been resolved in this moment, but will be the subject of our future investigations.

For the best detector No. 1217 we present our measurements of heterodyne signals for constant local oscillator power of 3 [W] and different signals power. As can be seen from Fig. 9, the minimum detectable power $(P_S)_{\min}$, defined as

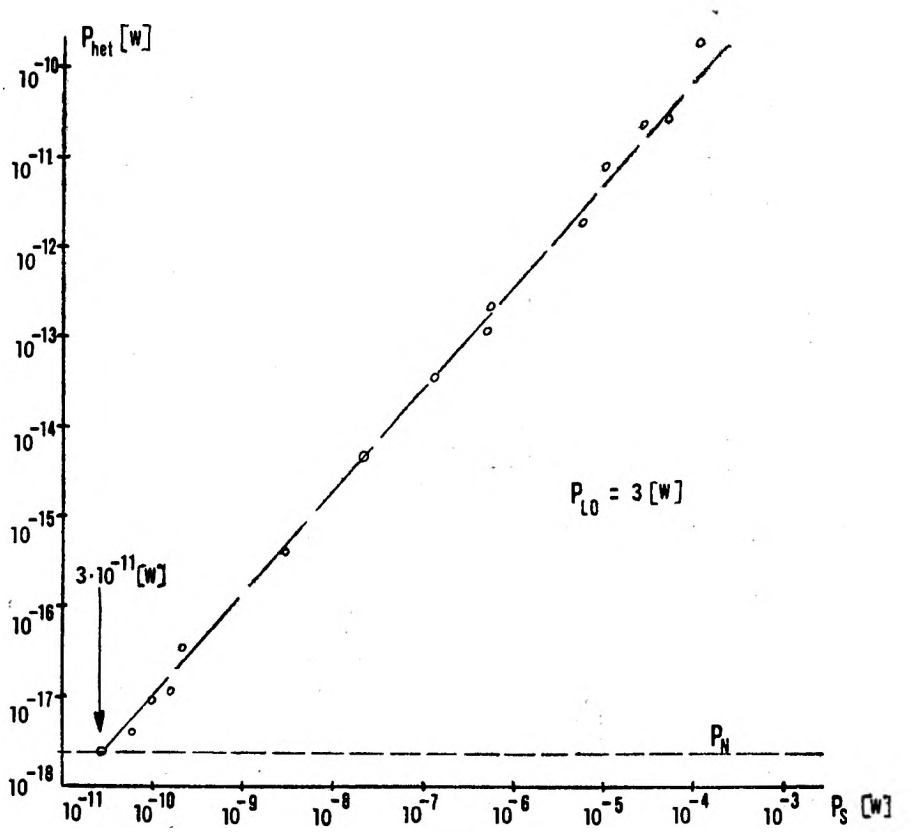

Fig. 9. Typical data points for detector No. 1217 for a given signal power and constant local oscillator power of 3 W

a signal beam power for which the heterodyne signal to noise power ratio is unity, was about 3×10^{-11} W. In a 1 Hz bandwidth this corresponds to a minimum detectable power of 6×10^{-18} [WHz^{-1}]. The experimental points presented in Fig. 9 are in good agreement with the data points and theoretical curve taken for step-decreased $P_S \times P_{LO}$ in slightly different experimental arrange-

ment. The value of $P_S \times P_{LO}$ of 7×10^{-11} W^2 corresponds, for $P_{LO} = 3$ W, to $(P_S)_{\min} = 2.3 \times 10^{-11}$ W.

In Figure 10 we present the signal to noise ratio, $(S/N)_{\text{power}}$, for N – amplifier noise, for different radii of beam spot on the detector area. The data were taken for various detector positions around the focus point of the L_2 lens in the

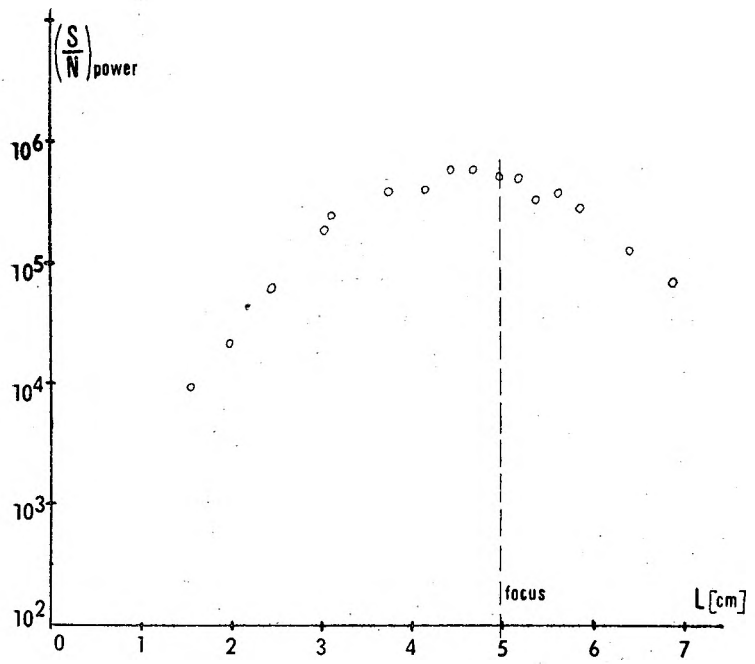

Fig. 10. Heterodyne power signal to noise ratio for various detector positions

arrangement shown in Fig. 4. It can be seen that the best detector position is nearly coincident with the focus point of the lens employed. It should be noted that another geometrical factor, i.e., angular alignment restriction, is about 20 times less stringent at 10.6 μm than in the visible region of the spectrum.

As indicated earlier, the roughness of the sandblasted wheel is comparable to the radiation wavelength λ. The bandwidth of the resulting noise modulation should be given by

$$B \sim v/d$$

where v is the velocity at which the illuminated spot transverses the surface and d is the diameter of the focussed spot on the wheel. This follows from the fact, that every d/v seconds a new spot on the wheel is illuminated, giving rise to scattered radiation which is uncorrelated with that of the previous time interval. Giving $v = r\dot{\theta}$ and $d \cong (F\lambda)/D$, we obtain approximately [3]

$$B \sim r\dot{\theta}D/F$$

where v — tangential velocity of the wheel, $\dot{\theta}$ — angular velocity of the wheel, r — radius of the wheel, F — focal length of the lens, D — diameter of the radiation beam in front of the lens.

Taking $r = 12.2$ cm, $\dot{\theta} = 20\pi/s^{-1}$, $D = 8$ mm, $F = 5$ cm, $\lambda = 10.6$ μm we obtain

$$B_n \sim 120 \text{ kHz},$$

which is comparable with the value observed with the Hewlett-Packard spectrum analyzer (Fig. 11).

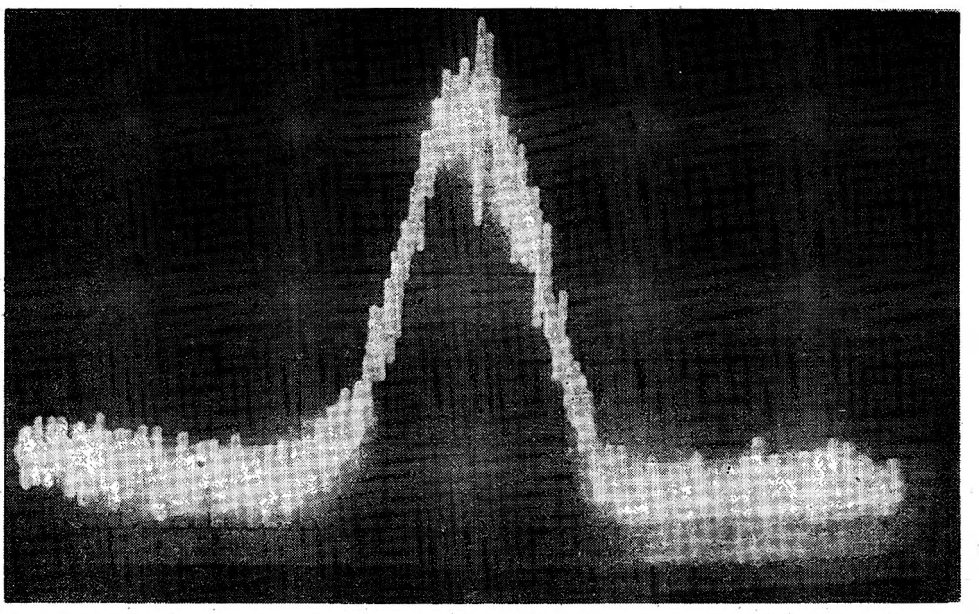

Fig. 11. A typical power spectral density trace of the heterodyne signal. Horizontal scale 0.05 MHz/div. The centre frequency is 0.7 MHz

In another simple experimental arrangement, shown in Figure 12, we have observed Doppler frequency-shifted return signals from the moving, diffuse-reflecting objects, for example, a slowly moving man. For a moderate local oscillator power of 0.3 W, signal power of 3 W and a distance of about 120 m, we have measured a signal to noise ratio of about 2. A typical Doppler shift was 160 kHz, which at 10.6 μm is equivalent to radial velocity of 3 km/h. It should be noted that we have not employed any transmitting-receiving telescope in this configuration.

The return signal power can be obtained from a simple range-finder equation (see, for example, [5]). In this experiment, the estimated value of P_S is about 1×10^{-10} W. On the other hand, taking the (S/N) experimental data, we can obtain P_S from Fig. 8. For $(S/N)_{\text{power}} = 2$ and $B = 5$ MHz, the value

of P_{het} is $P_{het} = 5 \times 10^{-18}$ WHz^{-1}. This is the point of $P_S \times P_{LO} = 1 \times 10^{-11}$ W^2, and for P_{LO} of 3 W, P_S will be 3×10^{-10} W.

For the maximum local oscillator power of 3 W, and a small, 5 cm diameter telescope, the estimated maximum range will be over 3000 m. In this estimation we assumed that only 1 W of laser power is transmitted to the target, the detection bandwidth of 0.3 MHz is the acceptable value for slowly moving objects, and that there is no attenuation of the signal beam in the atmosphere.

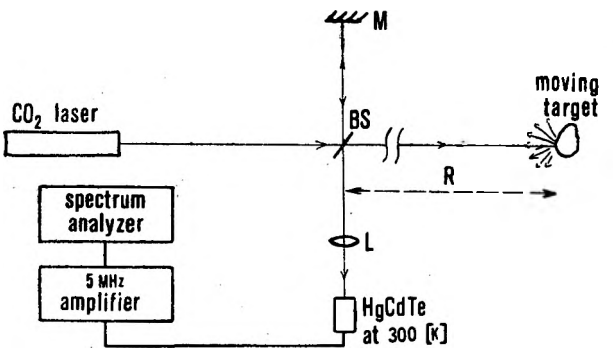

Fig. 12. Experimental arrangement for the heterodyne detection of moving objects outside the laboratory

4. Conclusions

It has been shown that heterodyne techniques are valuable in the infrared even for room-temperature detectors. It should be pointed out that coherent detection in the infrared is expected to be more sensitive than in the optical region because of the smaller photon energy.

Further improvements in heterodyne sensitivity may be expected since the quantum efficiencies of detectors such as HgCdTe photoresistors, which are presently $\eta = 0.1$, show promise of being greater in the furture. It is also possible to increase the local oscillator laser power (pulsed local oscillator) and/or to employ a high repetition pulsing detector supply. Then it will be possible to achieve near theoretical limit in infrared coherent detection.

Although the experimentally obtained value of minimum infrared signal power is two orders of magnitude larger than the theoretically attainable values for ideal cooled detector, the advantages and potential usefulness of room-temperature HgCdTe detectors for infrared heterodyne receivers has been demonstrated.

References

[1] KINGSTON R. H., *Detection of optical and infrared radiation*, Springer-Verlag, Berlin-Heidelberg-New York 1978.
[2] KEYES R. J., *Optical and infrared detectors*, Springer-Verlag, Berlin-Heidelberg-New York 1968.
[3] TEICH M. C., Proc. IEEE **56** (1968), 37.
[4] GALUS W., et al., Infrared Phys. **19** (1979), 649.
[5] GERRY FLOM, Appl. Opt. **11** (1972), 291.

Received July 13, 1983